ELSEVIER

Journal of Power Sources 81–82 (1999) 27–32

JOURNAL OF POWER SOURCES

www.elsevier.com/locate/jpowsour

Lithium silicon tin oxynitride (Li_ySiTON): high-performance anode in thin-film lithium-ion batteries for microelectronics

B.J. Neudecker *, R.A. Zuhr, J.B. Bates

Solid State Division, Oak Ridge National Laboratory, Oak Ridge, TN 37831-6030, USA

Abstract

A lithium-ion thin-film battery, consisting of the amorphous silicon tin oxynitride anode ('SiTON'), the amorphous lithium phosphorus oxynitride electrolyte ('Lipon'), and a crystalline $LiCoO_2$ cathode, can be heated at 250°C in air for 1 h which exceeds by far the required solder reflow conditions for electronic circuit assembly. Moreover, the performance of such a battery was found to even improve after the heat treatment. The Li_ySiTON profile between 0 and 1.2 V vs. Li was determined in $SiTON/Lipon/LiCoO_2$ lithium-ion thin-film cells equipped with a Li metal reference electrode. By comparison with a $Sn_3N_4/Lipon/LiCoO_2$ three-electrode lithium-ion thin-film cell, a model for the electrochemical insertion/extraction process of Li_ySiTON was suggested. The $SiTON/Lipon/LiCoO_2$ cells sustained 5 mA/cm^2 between 4.2 and 2.7 V while the anode supplied a reversible discharge capacity of about 340 μA h/mg or even 450 μA h/mg after heating at 250°C in air for 1 h. A long-term cycling stability test of a $SiTON/Lipon/LiCoO_2$ battery between 3.93 and 2.7 V demonstrated that the Li_ySiTON capacity faded only by 0.001% per cycle when charging was stopped as soon as the Li_ySiTON potential reached 0 V vs. Li. When this cathode-heavy cell was charged to 4.1 V (Li_ySiTON at 0 V vs. Li), a significantly higher reversible discharge capacity was obtained over ~5000 cycles.

Keywords: Silicon tin oxynitride (SiTON); Lithium-ion battery; Solder reflow; Microelectronics; Heat treatment; Hysteresis

1. Introduction

In recent years, higher densities and thermal management of microelectronic devices have made the solder reflow or surface mount technique a preferred method for assembling electronic circuits. Using this method, the predeposited solder bumps on the circuit board loaded with all of the unsoldered electronic components are heated to temperatures of up to 250°C in air or N_2 for less than 10 min. The thermal profile is highly board-specific and accounts for the melting point of the solder used and the package density of the board. A rechargeable battery, serving as an independent power supply or as a backup source in such electronic circuits, would be required to stand these conditions, since the integration of all of the components is preferably completed in one step only. In terms of a lithium-based rechargeable battery, these requirements preclude both the use of a lithium metal anode and the incorporation of a liquid organic electrolyte. To our knowledge, polymer electrolytes have not yet successfully been tested on their thermal stability in air at 250°C in contact with typical lithium-ion battery electrodes such as $LiCoO_2$, $LiNiO_2$, $LiMn_2O_4$, Li_yC, Li_yM (M = Al, Si, Sn, ...), $Li_4Ti_5O_{12}$, $Li_{3-y}Co_yN$, Li_ySnSiO_3, etc.

Recently, we demonstrated that a thin-film lithium-ion battery, consisting of the amorphous silicon tin oxynitride anode, 'SiTON' [1], the amorphous lithium phosphorus oxynitride electrolyte, 'Lipon' [2], and a crystalline $LiCoO_2$ cathode, exhibited excellent electrochemical properties even after heating the battery to 250°C in Ar for 1 h before the initial charge [3]. In this paper, we will show that such a battery can even be heated to 250°C for 1 h in air which proves our battery to be thermally stable in any industrial solder reflow process. 'SiTON' generally stands for $Si_aSn_bO_yN_z$ for $a+b=2$, $y \leq 4$, and $0 < z \leq 2.67$ and can adopt any composition within the prismatic phase diagram SiO_2–Si_3N_4–SnO_2–Sn_3N_4–Si–Sn by appropri-

* Corresponding author. Tel.: +1-423-241-4836; Fax: +1-423-574-4143; E-mail: 3bn@ornl.gov

0378-7753/99/$ - see front matter
PII: S0378-7753(98)00202-X

ately selecting the composition of the sputter target and the sputter gas atmosphere.

2. Experimental

Thin films with a stoichiometry of $SiSn_{0.87}O_{1.20}N_{1.72}$ and Sn_3N_4 were deposited by rf magnetron sputtering from a 2″-diameter glassy $SnSiO_3$ [4,5] target inside a graphite cast and a 2″-diameter Sn target, respectively, in N_2 at 20 mTorr. At a net applied rf power of 50 W, the deposition rate of $SiSn_{0.87}O_{1.20}N_{1.72}$ was about 35 Å/min, whereas Sn_3N_4 was deposited at a rate of 50 Å/min at 20 W. The as-deposited mass of these thin films was calculated from the deposition time and the steady-state deposition rate measured with a thickness monitor inside the deposition chamber before and after film preparation. The film stoichiometry of $SiSn_{0.87}O_{1.20}N_{1.72}$ and Sn_3N_4 was determined by Rutherford backscattering (RBS) using Be substrates which, due to their very small background contribution, facilitated the determination of the O/N ratio.

The rf magnetron sputter-deposited $LiCoO_2$ cathode and the basic fabrication steps of thin-film lithium batteries have previously been described [6]. In the lithium-ion cells, the lithium metal anode was replaced by a $SiSn_{0.87}O_{1.20}N_{1.72}$ or Sn_3N_4 thin-film anode covered with a 1000 Å thick Ti anode current collector. The anode area of 1 cm^2 was congruent with the $LiCoO_2$ cathode while the current collector had the shape of the lithium metal anode shown in [6]. The performance of the batteries was recorded at various current densities usually between 4.2 and 2.7 V with a charge cutoff condition of $< 1\ \mu A/cm^2$. For a selected battery, these tests were followed by heat treatment at 250°C in air. Heating and cooling rates were determined to be about 50°C/min by a thermocouple attached to the battery substrate. Before each heat treatment, the battery was discharged to 1.5 V, resulting in $Li_ySiSn_{0.87}O_{1.20}N_{1.72}$ and Li_xCoO_2 potentials of about 2.4 V and 3.9 V vs. Li, respectively. After each heat treatment, the battery was thermally equilibrated at 25°C before its post-treatment performance was recorded as described above. Three-electrode cells were equipped with a 1 μm × 1 mm^2 Li metal reference electrode embedded inside two sandwiching Lipon electrolyte layers of 0.75 μm thickness each. These cells were operated only at 25°C in an Ar atmosphere and were not subjected to heat treatment tests. The stoichiometric parameter y of $Li_ySiSn_{0.87}O_{1.20}N_{1.72}$ (='Li_ySiTON') was calculated based on the as-deposited anode mass of $SiSn_{0.87}O_{1.20}N_{1.72}$ and the galvanostatically inserted amount of lithium. The quasi-open circuit voltage profile ('q-OCV') of Li_ySiTON was recorded by galvanostatic intermittent titration of lithium into and out of the anode of a SiTON/Lipon/$LiCoO_2$ three-electrode cell equipped with a Li metal reference electrode where Li_ySiTON had already been cycled between 0 and 1.2 V vs. Li for 1000 times. Quasi-OCV data points were logged when the cell potential changed by less than 5 mV/h.

3. Results and discussion

In a lithium-ion thin-film battery of the construction SiTON/Lipon/$LiCoO_2$, the $LiCoO_2$ cathode not only serves as 615 the positive electrode but is also used as the initial lithium source. The initial cycle of such a battery is shown in Fig. 1 where the individual potentials of the anode and the cathode were independently monitored by the Li metal reference electrode. In this particular battery, anode and cathode were balanced in such a way that both electrodes cycled within their highly reversible voltage limits of 0–1.2 V vs. Li and 4.2–3.9 V vs. Li, respectively. This resulted in a battery voltage range of 4.2–2.7 V and a specific reversible discharge capacity of the anode of 475 μA h/mg which was maintained in the second cycle as shown in Fig. 2. As seen in Fig. 1, the irreversible formation of an X-ray amorphous Li–Si–Sn–O–N phase, which occurred in the SiTON matrix during the initial charge of the battery and whose exact stoichiometry is yet to be determined, consumed lithium and thereby diminished the reversible capacity of the battery. The percentage capacity loss was reduced when a higher $LiCoO_2$/SiTON mass ratio was used, which extended the utilization of the anode capacity at 0 V vs. Li. As previously demonstrated [1,3], this kind of capacity extension not only reduced the percentage capacity loss but also increased significantly the absolute discharge capacity of the anode to over 1300 μA h/mg at 750 $\mu A/cm^2$. More moderate cases of anode capacity extension at 0 V vs. Li will be discussed with the help of the '250°C-test' battery and the '13 000-cycles' cell presented below.

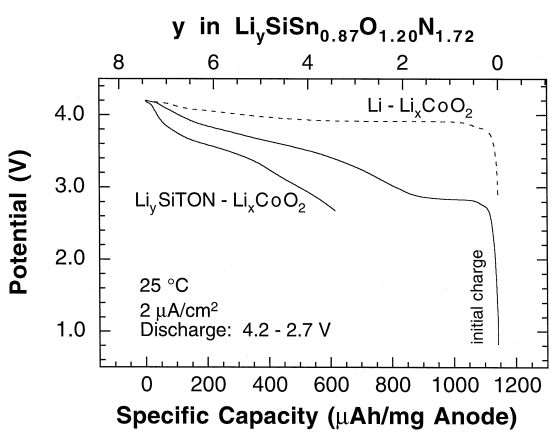

Fig. 1. Initial cycle of a three-electrode lithium-ion cell of the construction 1000 Å $SiSn_{0.87}O_{1.20}N_{1.72}$/1.5 μm Lipon/6000 Å $LiCoO_2$ equipped with a Li metal reference electrode. The monitored initial charge of the $LiCoO_2$ cathode vs. Li is included for comparison. Specific capacity based on the as-deposited anode mass.

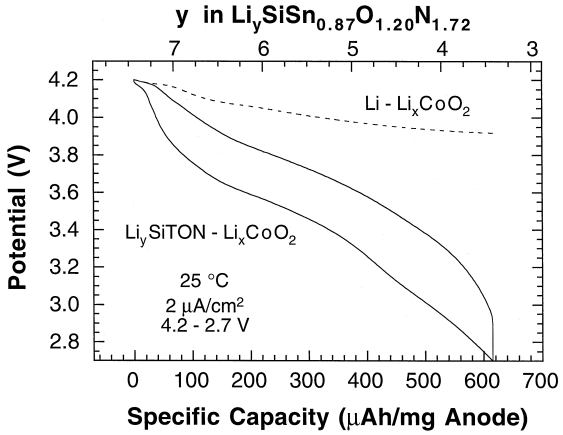

Fig. 2. The second cycle of the battery from Fig. 1. The Li–Li_xCoO_2 voltage profile is virtually the same for charge and discharge at 2 $\mu A/cm^2$.

The voltage profile of Li_ySiTON monitored by the Li reference electrode is shown in Fig. 3 and is identical with the profile that would have been obtained by simply subtracting the Li_ySiTON–Li_xCoO_2 profile from the Li–Li_xCoO_2 profile given in Fig. 2. Two questions, however, arise when scrutinizing the data shown in Fig. 3. (i) Can the insertion of only about 7.5 Li per $SiSn_{0.87}O_{1.20}N_{1.72}$ explain the observed anode potential of 0 V vs. Li? (ii) Why are the charge and discharge curves separated by more than 200 mV at the very low current density of 2 $\mu A/cm^2$ although the anode kinetics evidently were fast enough to sustain 5 mA/cm^2 while supplying 340 μA h/mg (see below)?

Estimated from the electrochemical measurements on the crystalline alloys Li_ySi [7,8] and Li_ySn [9], we expect the potential of $Li_ySiSn_{0.87}O_{1.20}N_{1.72}$ to approach 0 V vs. Li only if enough lithium is inserted into $SiSn_{0.87}O_{1.20}N_{1.72}$ so that the formal compositions $Li_{4.4}Si$ and $Li_{4.4}Sn$ are reached while creating a Li_2O/Li_3N phase. Because both Si and Sn are in valence state +4, $SiSn_{0.87}O_{1.20}N_{1.72}$ can be considered to consist formally of SiO_2, SnO_2, Si_3N_4, and Sn_3N_4 into which lithium is inserted according to the following reaction scheme:

$$SiO_2 + 8.4Li \rightarrow Li_{4.4}Si + 2Li_2O, \quad (1)$$

$$SnO_2 + 8.4Li \rightarrow Li_{4.4}Sn + 2Li_2O, \quad (2)$$

$$1/3Si_3N_4 + 8.4Li \rightarrow Li_{4.4}Si + 4/3Li_3N, \quad (3)$$

$$1/3Sn_3N_4 + 8.4Li \rightarrow Li_{4.4}Sn + 4/3Li_3N. \quad (4)$$

It is evident that 8.4Li per M (M = Si, Sn) are necessary to form $Li_{4.4}M$ regardless of how M may have initially been bonded to the oxygen or nitrogen ions in the glassy $SiSn_{0.87}O_{1.20}N_{1.72}$ anode. That is, in order to reach $Li_{4.4}Si$ and $Li_{4.4}Sn$, 15.7 ($= 1.87 \times 8.4$) Li per $SiSn_{0.87}O_{1.20}N_{1.72}$ would be needed, which is roughly twice as much lithium as read out from Fig. 3. This calculation suggests that only some M (M = Si, Sn) were alloyed in $Li_ySiSn_{0.87}O_{1.20}N_{1.72}$ while the remaining M was irreversibly trapped in the SiTON matrix. Direct evidence for any crystalline phase formation from in situ X-ray diffraction measurements could not be obtained, since $Li_ySiSn_{0.87}O_{1.20}N_{1.72}$ remained X-ray amorphous over the entire range of $0 < y < 7.5$.

In an attempt to apply the electrochemical information on the crystalline alloys Li_xM (M = Si, Sn) to $Li_ySiSn_{0.87}O_{1.20}N_{1.72}$, we treat, in a first approximation, $Li_ySiSn_{0.87}O_{1.20}N_{1.72}$ as a mixture of a crystalline Li_xM phase embedded in a glassy Li–M–O–N phase where two limiting cases may be considered: (i) only Li_xSi forms inside a Li–Sn–O–N phase or (ii) only Li_xSn forms inside a Li–Si–O–N phase. We further assume that $x \approx 0$ at 1.2 V vs. Li for both cases. Applying this model in Fig. 4, the superposition of the coulometric titration curves of the pure binary crystalline alloys Li_xSi [7,8] and Li_xSn [9] onto the Li_ySiTON profile of Fig. 3 suggests that Li_xSi was responsible for lithium insertion into Li_ySiTON below

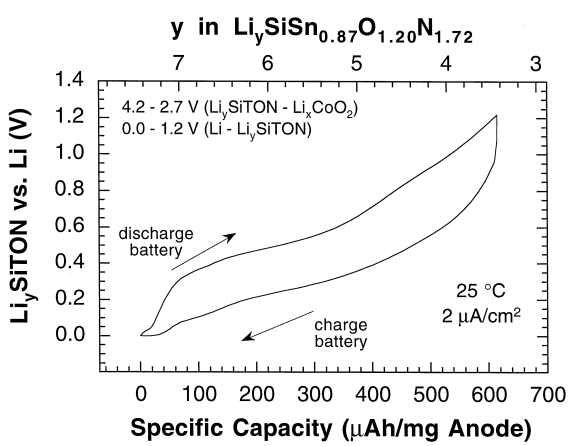

Fig. 3. The Li–Li_ySiTON voltage profile of the battery from Fig. 1.

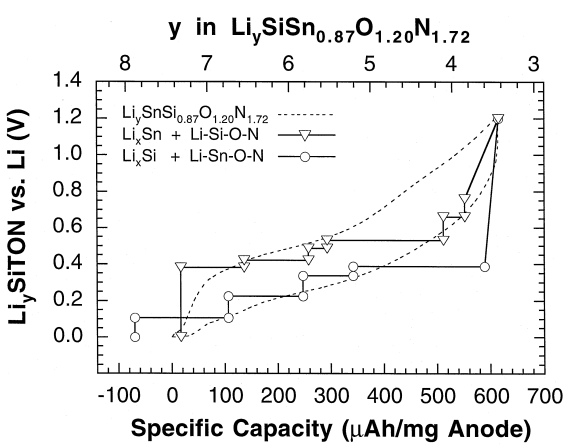

Fig. 4. Coulometric titration curves of crystalline Li_xSi (extrapolated to 25°C from Refs. [7,8]) and crystalline Li_xSn [9] superimposed on the Li_ySiTON voltage profile shown in Fig. 3 according to the model described in the text.

390 mV vs. Li whereas lithium extraction below 530 mV vs. Li occurred in Li_xSn. The deviation of the Li_ySiTON profile for $y < 5$ from the Li_xM (M = Si, Sn) titration curves may be understood in view of the amorphous character of Li_ySiTON which, instead of showing a step-like profile, could result in a sloping voltage profile as a function of the stoichiometric parameter y. In a different approach, the peaks in the differential capacity diagram of Li_ySiTON are compared in Fig. 5 to the potential and relative capacity of the two-phase plateaus of crystalline Li_xSi and Li_xSn. The figure suggests that Li_xSi may have contributed to the capacity of Li_ySiTON around 250 mV and 90 mV on charge as well as at 390 mV on discharge, whereas Li_xSn contributes to the capacity during lithium insertion between 380 and 660 mV.

In order to examine this idea of 'Li_xSi–Li_xSn separation', we prepared a three-electrode thin-film lithium-ion cell of the construction Sn_3N_4/Lipon/$LiCoO_2$ equipped with a Li metal reference electrode. The differential capacity diagram of $Li_ySn_3N_4$ vs. Li is shown in Fig. 6 together with the two-phase plateaus of the Li_xSn coulometric titration curve taken from Ref. [9]. The voltage profile of this cell should be dominated by Li_xSn, Li_3N, and perhaps Li–Sn–N thus, singling out these contributions to the voltage profile of Li_ySiTON. On lithium insertion, the $Li_ySn_3N_4$ anode was calculated to consist formally of $3Li_{4.4}Sn + 4Li_3N$ when reaching 0 V vs. Li, whereas on lithium extraction, the formal composition at 1.2 V vs. Li was $3Sn + 4Li_3N$. This clearly confirms Li_xSn to be the electroactive phase inside a mixed conducting $Li_{3\pm\delta}N$ phase whose practical decomposition voltage was determined to be higher than 1.2 V vs. Li [10]. By comparison of Fig. 6 with Fig. 5, we infer from the disappearance of the charge peak at 90 mV and the decreased shoulder at 390 mV on discharge that at these potentials, Li_xSi participated in the lithium insertion–extraction process during cycling of $Li_ySiSn_{0.87}O_{1.20}N_{1.72}$. However, the charge peak at 250 mV, which in Fig. 5 was assumed to stem from Li_xSi, remained in the differential capacity diagram of $Li_ySn_3N_4$ (Fig. 6), although at this potential, neither a large capacity region of Li_xSn [9] nor of $Li_{3\pm\delta}N$ [10] exists.

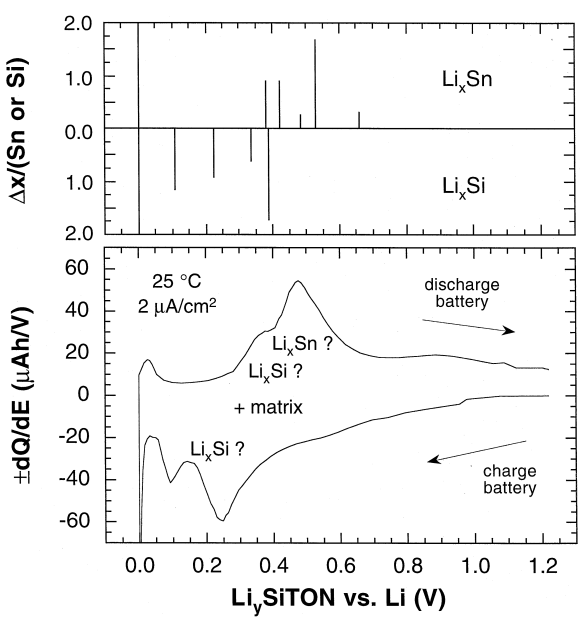

Fig. 5. Differential capacity diagram from the voltage profile in Fig. 3. The potentials and capacities of the two-phase plateaus of the binary, crystalline Li_xM alloys (M = Si, Sn) [7–9] are indicated in the upper plot.

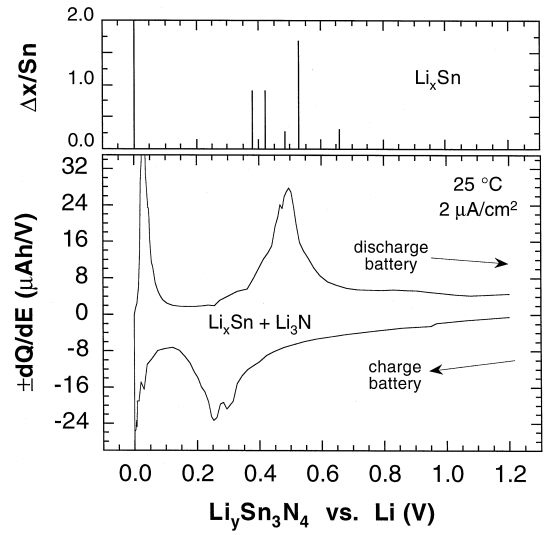

Fig. 6. Differential capacity diagram of $Li_ySn_3N_4$ monitored by the Li metal reference electrode of a Sn_3N_4/Lipon/$LiCoO_2$ three-electrode lithium-ion thin-film cell. The potentials and capacities of the two-phase plateaus of the binary, crystalline Li_xSn alloys [9] are indicated in the upper plot.

Thus, we conclude from the 200–250 mV gap between the charge and the discharge peaks seen in Figs. 5 and 6 and from the 250–350 mV gap between the charge and discharge profiles for a given lithium stoichiometry y in Fig. 3 that Li_ySiTON shows a true hysteresis on cycling. This also became evident in the 'q-OCV' profile of Li_ySiTON shown in Fig. 7 where fitting the voltage relaxation to a logarithmic time dependence and extrapolating to 40 days or even 10 years still produced a lithium-insertion profile that was separated by more than 100 mV from the lithium-extraction profile over most of the titration range. Such a phenomenon has also been observed in our amorphous cathodes $Li_xMn_{2-y}O_4$ for $0.22 \le y \le 0.33$ and $Li_xV_2O_5$ [11] and is believed to be caused by metastable domains inside the electrode which are sensitive to the direction of lithium transfer.

The rate capability of a 500 Å $SiSn_{0.87}O_{1.20}N_{1.72}$/1 μm Lipon/6000 Å $LiCoO_2$ lithium-ion battery before the heat treatment of 250°C in air is shown in Fig. 8. It is noticed that the battery was capable of sustaining high current densities of up to 5 mA/cm^2 while, based on the as-deposited anode mass 340, supplying about 260 μA h/mg

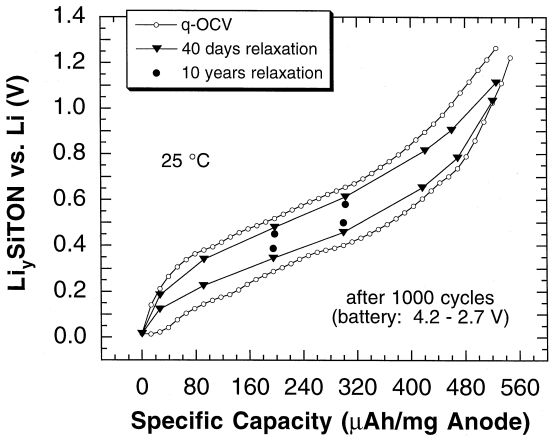

Fig. 7. Quasi-open circuit voltage profile ('q-OCV') of Li_ySiTON monitored by the Li metal reference electrode of a three-electrode lithium-ion cell of the construction 1000 Å SiTON/1.5 μm Lipon/5500 Å $LiCoO_2$ after the cell had been cycled for 1000 times where Li_ySiTON was 0–1.2 V vs. Li. The voltage relaxation after each titration step could be fitted to a logarithmic time dependence which was extrapolated to 40 days and 10 years.

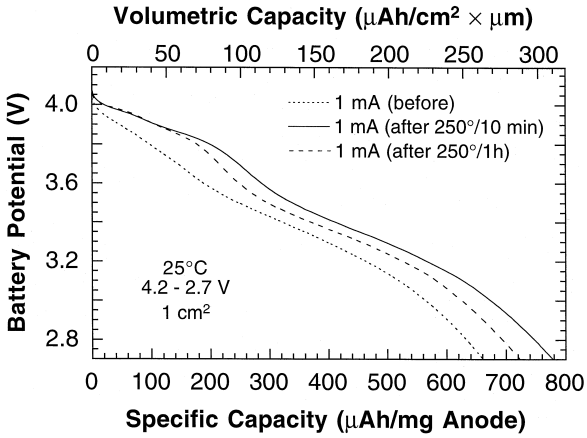

Fig. 9. Discharge profiles at 25°C of the battery from Fig. 8 before and after heating at 250°C in air for 10 min or 1 h. Specific capacity based on the as-deposited mass of SiTON and volumetric capacity calculated from the as-deposited SiTON volume.

reversible discharge capacity in the practical voltage range of 4.2–2.7 V.

As shown in Fig. 9, after heating at 250°C in air for 10 min, the reversible discharge capacity of the 500 Å $SiSn_{0.87}O_{1.20}N_{1.72}$/1 μm Lipon/6000 Å $LiCoO_2$ battery at 25°C increased by 10%, suggesting that a solder reflow process could even improve the performance of SiTON/Lipon/$LiCoO_2$ batteries. Such an improvement is probably brought about by the slightly increased ionic conductivity of the Lipon electrolyte after the treatment, as was confirmed in a separate test on a Pt/Lipon/Pt cell, and possibly by a reduced charge transfer at the solid-state electrolyte–electrode interfaces. As also noticed from Fig. 9, the $Li_ySiSn_{0.87}O_{1.20}N_{1.72}$ anode supplied 780 μA h/mg at 1 mA/cm^2, based on the as-deposited anode mass. On the charge half-cycles, about 25% of the lithium was returned to the anode at a potential of 0 V vs. Li.

Since in separate tests SiTON/Lipon/$LiCoO_2$ batteries did not deteriorate upon discharge to 1.0 V, we cycled the 500 Å $SiSn_{0.87}O_{1.20}N_{1.72}$/1 μm Lipon/6000 Å $LiCoO_2$ battery after the heat treatment test (250°C in air for 1 h) at rates of up to 20 mA/cm^2 in the voltage range 4.2–1.0 V at 25°C. We see from Fig. 10 that more than 200 μA h/mg were still supplied at 20 mA/cm^2, although the discharge voltage range only extended from 1.45 to 1.0 V. The discharge capacity at 10 mA/cm^2, however, was delivered in the more useful potential range of 2.8–1.0 V. As seen in Fig. 10, the specific discharge capacity between 4.2 and 2.7 V at 5 mA/cm^2 increased by 30% from 340 μA h/mg before the heat treatment to 450 μA h/mg after heating at 250°C in air for 1 h.

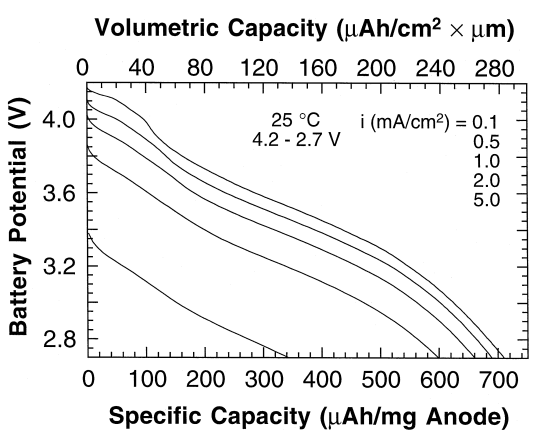

Fig. 8. Rate capability of a 500 Å SiTON/1 μm Lipon/6000 Å $LiCoO_2$ lithium-ion cell. Specific capacity based on the as-deposited mass of SiTON and volumetric capacity calculated from the as-deposited SiTON volume.

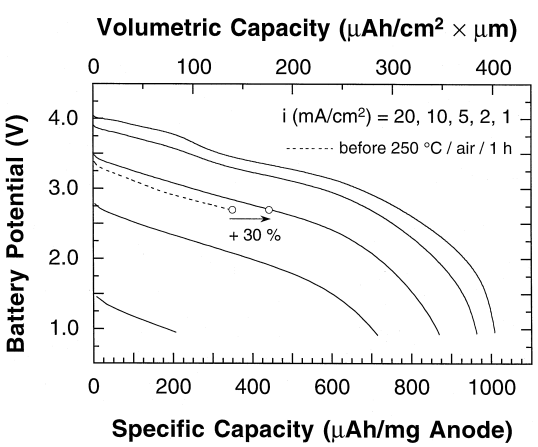

Fig. 10. High-rate capability test between 4.2 and 1.0 V at 25°C of the battery given in Fig. 9 after the heat treatment at 250°C in air for 1 h. The improved performance of the cell after heating is indicated by comparison with the 5 mA/cm^2 profile before the treatment taken from Fig. 8. Specific capacity based on the as-deposited mass of SiTON and volumetric capacity calculated from the as-deposited SiTON volume.

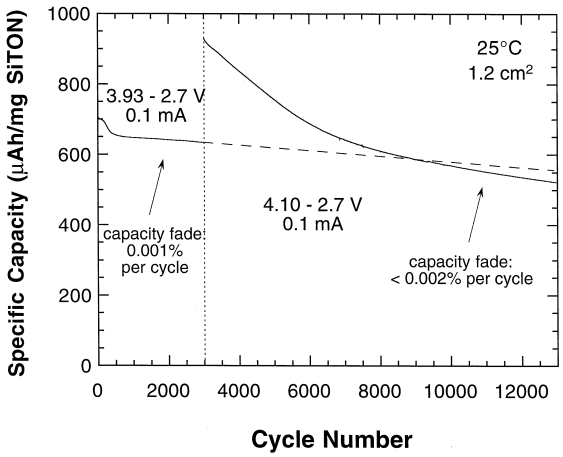

Fig. 11. Long-term cycling stability of a 100 Å SiTON/1.5 μm Lipon/2000 Å $LiCoO_2$ three-electrode lithium-ion cell with (4.1–2.7 V) and without (3.93–2.7 V) anode capacity extension at 0 V vs. Li. The dashed line extrapolates the anode without capacity extension to higher cycle numbers. Specific capacity based on the as-deposited mass of SiTON and volumetric capacity calculated from the as-deposited SiTON volume.

The long-term cycling stability of a 1.2 cm^2 large three-electrode lithium-ion battery of the construction 100 Å SiTON/1.5 μm Lipon/2000 Å $LiCoO_2$ equipped with a Li metal reference electrode is shown in Fig. 11. This cell was fabricated cathode-heavy as enough lithium was intended to be available to significantly extend the anode capacity at 0 V vs. Li without overcharging the Li_xCoO_2 cathode to values of x below 0.5. During the first 3000 cycles, the cutoff voltage on charge was set to 3.93 V where the Li_ySiTON anode just reached 0 V vs. Li. In this 3.93–2.7 V window, a very small capacity fade of about 0.001% per cycle was observed between cycle 400 and 3000. After 3000 cycles between 3.93 and 2.7 V, the charge cutoff voltage was raised to 4.1 V which increased the discharge capacity of the Li_ySiTON anode by almost 50% to 930 μA h/mg. Monitored by the Li reference electrode, this excess capacity was obtained at a potential of 0 V vs. Li and accounted for 1/3 of the entire Li_ySiTON capacity. However, it is not clear how much of this excess capacity resulted from plated or nucleated as Li metal, since this process is assumed to set in only after the lithium insertion capacity of both Li_xSi and Li_xSn inside Li_ySiTON has been exhausted. As discussed above for Figs. 3 and 4, this is obviously not the case when Li_ySiTON just reaches 0 V vs. Li. The capacity extension demonstrated in Fig. 11 proved to be very useful from cycle number 3000 to 8000 as evidenced by comparison with the extrapolated 3.93–2.7 V capacity curve.

4. Conclusions

A lithium-ion thin film battery of the construction SiTON/Lipon/$LiCoO_2$ shows no degradation in performance after heating at 250°C in air for 10 min to 1 h which by far exceeds the required solder reflow conditions for electronic circuit assembly. Such a battery also exhibits an excellent rate capability of up to 10 mA/cm^2 in a useful voltage range at 25°C. The capacity fade of 'SiTON batteries' is very low although the voltage window of the Li_ySiTON anode ranges from 1.2 to 0 V vs. Li where up to 1/3 of the entire Li_ySiTON capacity may be charged at 0 V vs. Li.

Probably, Li_xSn and Li_xSi are the electroactive domains within the amorphous matrix consisting of Li–Si–Sn–O–N. On charge, Li_ySiTON reaches 0 V vs. Li long before all of the Si and Sn atoms are formally alloyed to $Li_{4.4}M$ (M = Si, Sn). It is not yet clear at what state of charge Li metal actually plates onto or nucleates inside the Li–Si–Sn–O–N matrix.

Acknowledgements

This research was supported by The Department of Energy's Division of Materials Sciences, Division of Chemical Science, Office of Energy Research Technology Transfer Program, and Office of Transportation Technologies under Contract No. DE-AC05-96OR22464 with Lockheed Martin Energy Research.

References

[1] B.J. Neudecker, J.B. Bates, U.S. Pat. Appl. 09/057,147.
[2] X. Yu, J.B. Bates, G.E. Jellison Jr., F.X. Hart, J. Electrochem. Soc. 144 (1997) 524.
[3] B.J. Neudecker, R.A. Zuhr, J.B. Bates, Meeting Abstracts 97-2, Abstract No. 295, The Joint International Meeting, Aug. 31–Sept. 5, 1997, Paris, France.
[4] J. Carbó Nóver, J. Williamson, Phys. Chem. Glasses 8 (1967) 164.
[5] T. Ishikawa, S. Akagi, Phys. Chem. Glasses 8 (1978) 108.
[6] B. Wang, J.B. Bates, F.X. Hart, B.C. Sales, R.A. Zuhr, J.D. Robertson, J. Electrochem. Soc. 143 (1996) 3203.
[7] R.A. Sharma, R.N. Seefurth, J. Electrochem. Soc. 123 (1976) 1763.
[8] C.J. Wen, R.A. Huggins, J. Solid State Chem. 37 (1981) 271.
[9] J. Wang, I.D. Raistrick, R.A. Huggins, J. Electrochem. Soc. 133 (1986) 457.
[10] O.V. Zheltonozhko, V.P. Obrosov, N.N. Batalov, Soviet Electrochem. 28 (1992) 183.
[11] N.J. Dudney, J.B. Bates, F.X. Hart, Meeting Abstracts 96-2, Abstract No. 877, 190th Electrochemical Society Meeting, Oct. 6–11, 1996, San Antonio, TX.